*Journal of the Society of Automotive Engineers Malaysia*
*Volume 2, Issue 2, pp 112-126, May 2018*
*e-ISSN 2550-2239 & ISSN 2600-8092*

# Numerical Simulation of Combustion Behavior of DI Diesel Engine with Conjunction of AMR and Embedding Refinement Strategies

K. Naima[*1], A. Liazid[2] and H. Bousbaa[2]

[1]University Center of Nâama BP 66, Nâama, Algeria
[2]Research Laboratory LTE-ENPO, B.O. 1523 El Mnaouer 31000 - Oran, Algeria

[*]*Corresponding author: n_khatir@hotmail.com*

**ORIGINAL ARTICLE** **Open Access**

**Article History:**

Received
*27 Dec 2017*

Received in revised form
*22 March 2018*

Accepted
*6 April 2018*

Available online
*1 May 2018*

**Abstract** – *Currently, computational fluid dynamics has become an effective supplement to experimentation in the analysis and development of various engineering systems including internal combustion engines. In fact, multi-dimensional modelling of IC engines is less extensive and less time consuming than experimentation. In this aim, CONVERGE code was used to study the combustion behavior in a DI engine with various mesh control techniques including embedding and Adaptive Mesh Refinement (AMR). The simulation covers the compression, spray, combustion and expansion. A single spray plume and 1/6th of the combustion cylinder (60 degrees) is simulated. In light of the simulation results it is extremely recommended to use AMR approach in conjunction with embedding around the nozzle for running engine simulations.*

**Keywords:** CFD, internal combustion engine, grid control, AMR


*Journal homepage: www.journal.saemalaysia.org.my*

## 1.0 INTRODUCTION

In recent decades, total worldwide energy consumption has been increased significantly. It leads to the global warming phenomenon resulting in higher average temperature of the earth (Masoudi & Zaccour, 2017) and threatening the energy security (Wallington et al., 2013). According to International energy agency rate of energy consumption will increase by 53% in 2030 (Ong et al., 2011). Because of the growth of diesel engine population, there is an increasing demand for engine fuels (Jiaqiang et al., 2017).

Diesel engines are extensively used in all types of transportation sectors due to their improved durability and efficiency (Jiaqiang et al., 2017). However, nearly 30% of the world's greenhouse gas emissions are produced from the transportation sector, leading to global warming (Geng et al., 2016). Meanwhile, diesel engines are the major sources of inhaled air-suspended particulate matters (Frigo et al., 2014) (Kalargaris et al., 2017). In this context the combustion of diesel engines needs to be studied and improved to increase efficiency and reduce emissions.

Researches community have realized that the development of designs and performances of systems involving combustion cannot rely solely only on experimentations. The rapid progress in the computing systems coupled with the availability of a wide range of CFD codes, makes it possible to simulate complex turbulent combustion flows with complex geometries within reasonable time. This has made CFD a practical adjunct to experimentation allowing consequently a deep verification and exhaustive interpretation of experimental results (Amsden & Amsden, 1993). More recently, a growing number of publications (Atmaca et al., 2016; Guo et al., 2018; Jafari et al., 2016; Li et al., 2017; Maurya & Mishra, 2017; Pandal et al., 2018; Petranović et al., 2017; Sideri et al., 2017; Silva et al., 2017; Soni & Gupta, 2016) focusing on the use of CFD codes to extensively investigate the combustion behavior of ICE have been carried out. However, a key problem for these studies dealing with numerical simulation of engine's combustion is how to adjust more accurately the CFD code.

The good agreement between the numerical and experimental pressure curves is stated when the error between them is smallest. Hence, the choice of the numerical models, the appropriate meshing process and refinement strategies should be adequate. Although extensive researches have been carried out using CFD, much of the current literature pays particular attention to the combustion and emissions analysis. The Lack of refinement process can lead to underprediction of combustion and emissions characteristics. The following examples carried out recently without any mesh refinement strategies show a contrast between measured and experimental results.

For example, Soni and Gupta (2016) studied the optimization of methanol powered diesel engine with a CFD approach. The authors performed a grid independency test to choose the appropriate mesh (independency of grid size) from three mesh sizes with 29516, 40868 and 50208 cells. The optimum mesh size with 40868 cells is considered. This grid takes roughly 6 hours of simulation time. The gap between the experimental and numerical in-cylinder pressure was in the range of 3-4 bar.

Guo et al. (2018) conducted an experimental and CFD investigation to explore the effect of fuel injection characteristics on the performance of a diesel engine. To simulate the combustion characteristics, a dynamic mesh is adopted. The total mesh cells are 70686 cells. The size of the cells is set 4 times of nozzle diameter without giving further details about this diameter. A difference of 3.5 bar is observed between the experimental and numerical in-cylinder pressures.

Maurya and Mishra (2017) performed a numerical parametric study on a four-stork dual fuel engine with a CFD approach to analyse the combustion performances and emissions characteristics of port injected natural gas and diesel pilot injection. The computational mesh contains 88878 cells without any refinement process and represents one fourth of entire cylinder chamber. The simulation takes several hours from -20 CAD BTDC to +40 ATDC. The deviation between the measured and computed pressure is 3.5 bar.

Even though the mentioned papers are consistent with high scientific value, the numerical simulation results could be further enhanced if the authors would take advantages of the refinement strategies. Within this context, the purpose of this investigation is to show the benefits of using both AMR and embedding refinement strategies to help future searchers in this area to address accuracy within reasonable computational time.

## 2.0 COMPUTATIONAL TECHNIQUE AND MODEL DESCRIPTION

The program used in the current study is CONVERGE CFD code (Richards et al., 2008). This multi-dimensional program is developed for various engineering applications including internal combustion engine simulation (Bousbaa et al., 2012; Huang et al., 2016; Khatir & Liazid, 2013; Ndayishimiye et al., 2011). The geometry surface is immersed within a Cartesian block. The cells are trimmed by the intersecting surface, after which the intersection information (e.g., surface areas, normals, etc.) is reduced before being stored for each cell. This allows for complex surface intersection to be more easily represented for simulation (Richards et al., 2008).

## 3.0 COMPUTATIONAL FRAMEWORK AND GRID CONTROL STRATEGIES

### 3.1 Grid Refinement

A numerical model for Caterpillar 3401 direct injection is represented with a computational mesh representing $1/6^{th}$ of the total combustion chamber. The specifications of the engine are shown in Table 1.

**Table 1**: Engine parameters

| Engine Parameter | Value |
|---|---|
| Bore | 13.716 cm |
| Stroke | 16.51 cm |
| Connecting rod length | 26.3 cm |
| Squish | 0.4221 cm |
| Displacement | 2.44 L |
| Compression ratio | 15.1:1 |
| Nozzle hole diameter | 0.026 mm |
| Intake surge tank pressure | 183 kPa |
| Intake surge tank temperature | 309 K |
| Intake valve closure | -147 CAD ATDC |
| Swirl Ratio (nominal) | 0.98 |
| Engine speed | 1600 rpm |
| Mass of fuel injected | 0.1621 g/cycle (all six holes) |
| Injection duration | 21 degrees |
| Load | 75% |
| Indicated power | 26.64 kW |
| Start of injection | -9 CAD BTDC |
| Injection temperature | 341 K |

At the beginning of the simulation, cell size is set to 2 mm in x, y and z directions. Grid embedding is also used to control the mesh and allows adding grid resolution locally in critical flow sections of the domain and leaves less critical sections of the domain coarse (Figure 1). In the current study embedding technique for both boundary and nozzle was used to resolve spray and wall effects. Figure 2 shows the grid embedded for nozzle and boundary.

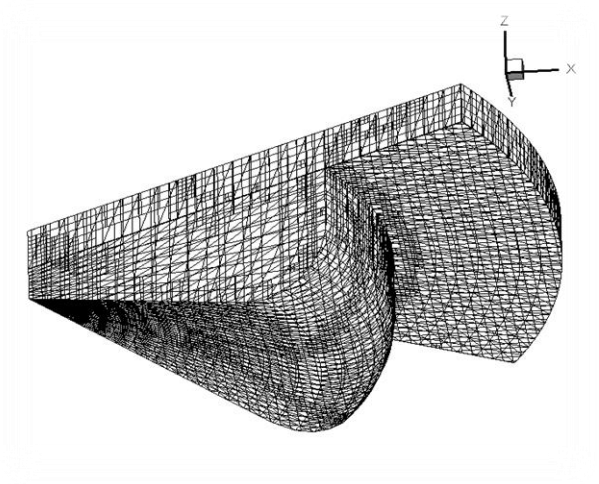

**Figure 1:** Computational mesh at +10 CAD ATDC

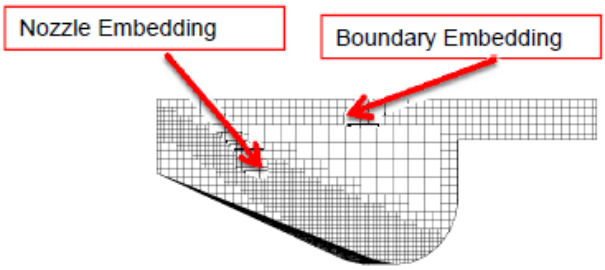


**Figure 2:** Embedding around the boundary and nozzle

Another refinement technic based on AMR (Adaptive Mesh Refinement) is used. AMR enhances the mesh resolution automatically based on gradients in field variables (temperature, pressure, etc.). AMR is used for temperature because it ensures a higher grid resolution where the temperature gradient is highest.

### 3.2 Spray Model

The experiment fuel is a diesel fuel; however, a surrogate fuel (C14H30) is used in this study. A surrogate fuel is used because Diesel fuel contains many different chemical compounds and thus to simplify the calculation a single compound is chosen.

The thermophysical properties of the liquid fuel (density, viscosity, surface tension, latent heat of vaporization, vapour pressure, conductivity, and specific heat) are strongly dependent on temperature. A prior determination of the change of the thermophysical properties with temperature is very important for spray calculation (injection, breakup, collision, vaporization, etc.). For the liquid injection a Blob cone injection model is used. The appropriate rate shape is as shown in Figure 3 and 4. An accurate determination of the drop drag coefficient is critical for an accurate spray modelling, for this aim the dynamic drag model is used because it allows determining the droplet drag coefficient dynamically. In order to model the spray breakup a modified KH-RT model is used. This model refers the primary breakup of the injected liquid blobs to the aerodynamic instabilities commonly known as Kelvin-Helmholtz waves. For the collision and coalescence modelling the NTC (No Time

Counter) model is used. The NTC method is based on techniques used in the gas dynamics for DSMC (Direct Simulation Monte-Carlo). This model has been shown to be faster and more reliable (Richards et al., 2008).

### 3.3 Combustion an Emissions Models

The experiment fuel is a diesel fuel; however, a surrogate fuel (C14H30) is used in this study. A surrogate fuel is used because Diesel fuel contains many different chemical compounds and thus to simplify the calculation a single compound is chosen.

The shell/CTC is a widespread model for diesel combustion modelling due to its clearness, understandability and sufficient accuracy (Lakshminarayanan & Aghav, 2010; Shi et al., 2011). The model involves two sub-models: CTC and shell. The CTC model handles the conversion rate of the density of species at high temperature reactions while Shell models the auto ignition process of diesel fuel (Halstead et al., 1977). Shell was primarily elaborated to predict knock in spark ignition engines. This model uses a simplified reaction mechanism to simulate Auto ignition in diesel engines. This model contains eight reactions given by:

$$\begin{aligned} &C_nH_{2m} + O_2 \rightarrow 2R^* \\ &R^* \rightarrow R^* + P + Heat \\ &R^* \rightarrow R^* + B \\ &R^* \rightarrow R^* + Q \\ &R^* + Q \rightarrow R^* + B \\ &B \rightarrow 2R^* \\ &R^* \rightarrow Termination \\ &2R^* \rightarrow Termination \end{aligned} \tag{1}$$

The characteristic time-scale combustion model (CTC) model is used for high temperature combustion (Abraham et al., 1985; Xin et al., 1997). CTC models the rate of change of the density of species *m*, $\rho$, as:

$$\frac{\partial \rho_m}{\partial t} = -\frac{\rho_m - \rho_m^*}{\tau_c} \tag{2}$$

Where $\rho^*$ is the local and instantaneous thermodynamic equilibrium value of the species density and $\tau_c$ is the characteristic time to achieve equilibrium. The characteristic time is calculated via:

$$\tau_c = \tau_{chem} + f\tau_{turb} \tag{3}$$

Where $\tau_{chem}$ is the chemical-kinetics time, $\tau_{turb}$ is the turbulent mixing time and $f$ is a delay coefficient which simulates the increasing influence of turbulence on combustion. The chemical timescale is modelled as follow (Kong et al., 1995):

$$\tau_{chem} = \frac{[C_nH_{2m}]^{0.75} e^{\frac{E_{chem}}{R_u T_g}}}{2A_{chem}[O_2]^{1.5}} \tag{4}$$

Where $A_{chem}$ is a constant. $E_{chem}$ is the activation energy given by 18475 *cal/mol*. $R_u$ is the universal gas constant and $T_g$ is the gas temperature. In addition, the turbulent timescale is given as:

$$\tau_{turb} = C_2 \frac{k}{\varepsilon} \quad (5)$$

Where $C_2$ is a constant. For soot and $NO_x$ production Hiroyasu soot model and Zeldovich $NO_x$ model were respectively used.

### 3.4 Turbulence Model

The rapid distortion RNG k-ε model is used. This model is designed for rapid compression or rapid expansion; therefore, it is commonly used for ICE simulation. Han and Reitz (1995) Demonstrated the efficiency of this model for spray injection modelling. In fact, the spray generates a mean flow gradient which is responsible for the enhancement of turbulent to mean-strain time scale ratio. In addition, Han and Reitz heat transfer wall model is used.

## 4.0 RESULTS AND DISCUSSION

The simulation was achieved in a three dimensional in-cylinder computational mesh. This mesh represents one-sixth of the engine combustion chamber for a base cell size of 2 mm. In this simulation AMR embedding scale of 2 is set for the spatial gradient in the temperature which gives a minimum cell size of 0.5mm. The total cells at the start of the simulation is 58096. Figure 5 gives the evolution of the number of cells in the computational domain with CAD. An example of 2 mm base mesh with refinement at +37 CAD ATDC is illustrated in Figure 6. The maximum cells provided with AMR is around 370000 cells at +37 CAD ATDC (Figure 6-a). At this time (+37CA ATDC) the flame takes the largest volume on the computational domain (Figure 6-b).

The simulation was performed on 5 cores and took approximately 18.83 hours. 77.73% of this time is used for solving the transport equations, while 16.29% is used to move surface and update grid.

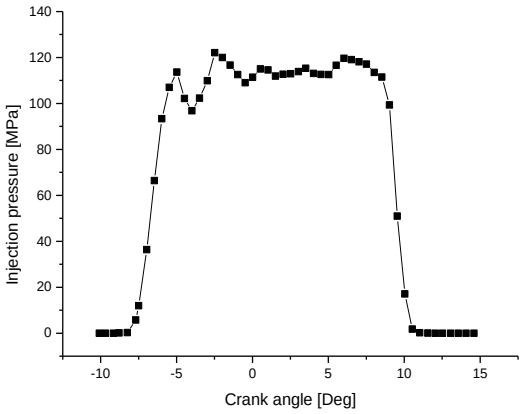


**Figure 3:** Injection profile

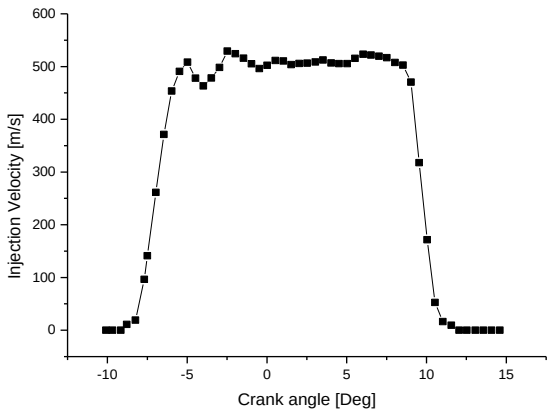


**Figure 4:** Injection velocity

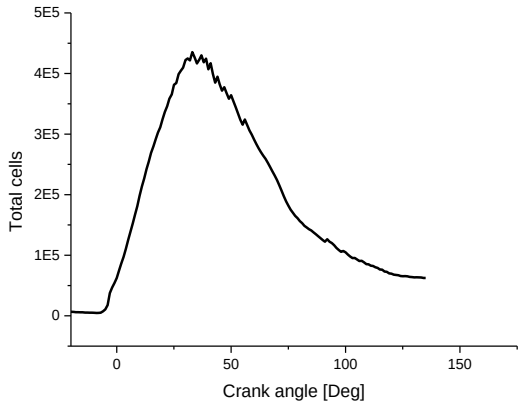


**Figure 5:** Total cells in the computational domain

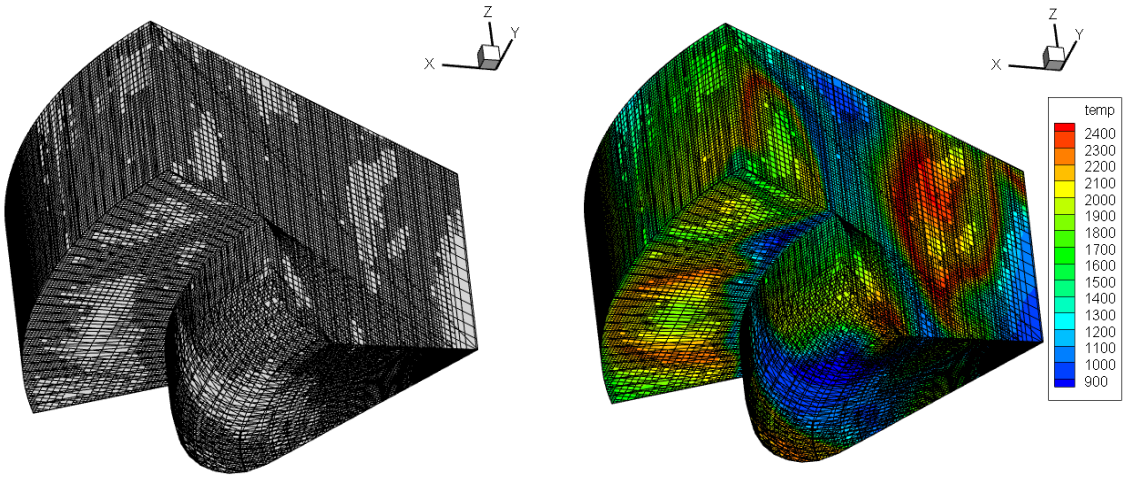


**Figure 6:** Computational domain at +37 CAD ATDC: (a) without contours; (b) with temperature contours

Fuel is injected under high pressure at -9 CAD BTDC into the main combustion chamber with a central hole nozzle. High injection pressure (Figure 3) and the small hole nozzle lead to a good mixture formation. The shape of the bowl allows the spray to penetrate much longer into the combustion chamber and gives it a sufficient time to evaporate and to mix with air. At the same time the bowl avoids the injected fuel to collide with the wall.

Figure 7 shows the computed and experimental in-cylinder pressure (Montgomery & Reitz, 1996; Xin et al., 1997). A good agreement between numerical and experimental in-cylinder pressure is obtained. The zoomed view of Figure 7 shows a slight underprediction in the pressure around the TDC. The underprediction of the pressure may be due to the mechanism involved in the mixture formation and the spray atomization which may result in a slight reduction in the temperature due to the absorption of heat during compression. The overprediction showed in the zoomed view of Figure 7 may be due to RNG k- ε model which apparently misrepresent the rate of mixing during combustion. (Huang et al., 2016).

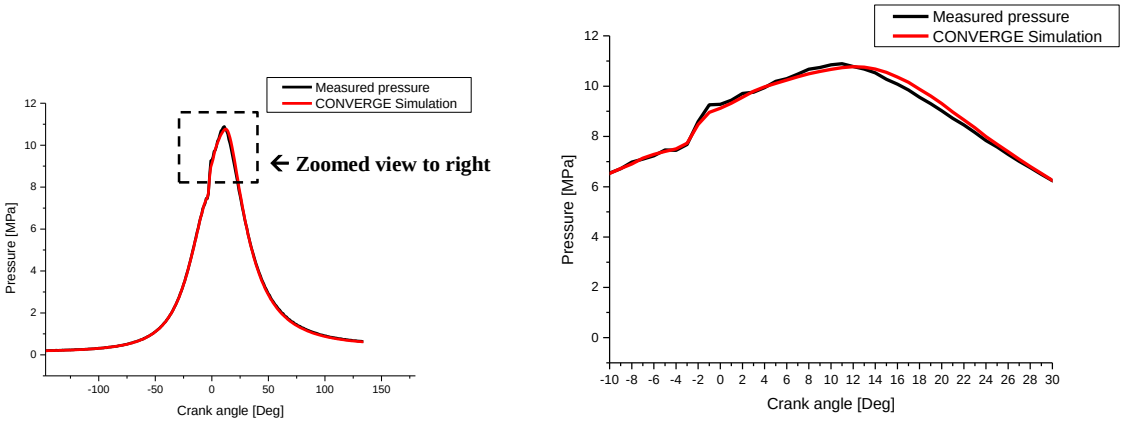


**Figure 7:** In-cylinder pressure evolution (experiment and CONVERGE simulation)

Figure 8 depicts the heat release rate evolution from -20 CA BTD to +40 CA ATDC. Generally, heat release rate of the diesel engine is subdivided into four phases: The ignition delay period, which is commonly defined as the period between start of fuel injection and the start of combustion. The second phase is the premixed combustion, in which the homogenous air/fuel mixture is brought into the flammability limits and burns rapidly in a few crank angle degrees resulting in a high heat release rate. The next phase is mixing controlled combustion. The burning rate is controlled by the fuel vapour air mixing process. In this phase the heat release rate may not reach another peak, it decreases as this phase progresses (Heywood, 1988). The last phase is post-combustion or late combustion phase where in-cylinder pressure and temperature decrease significantly and the combustion is controlled by reaction kinetics.

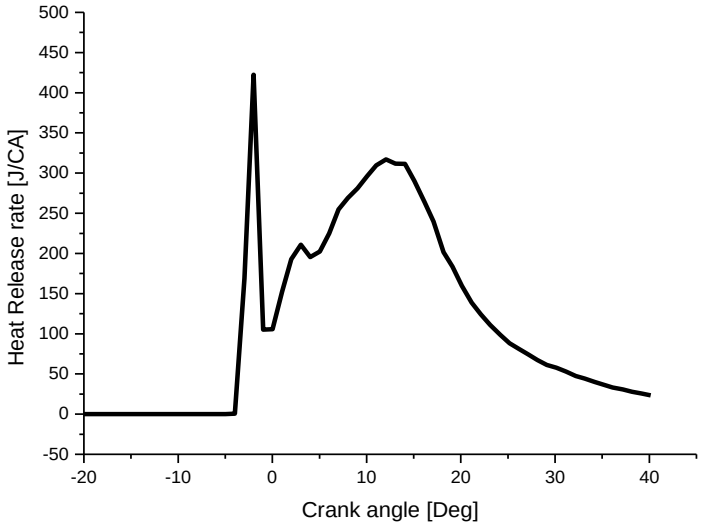


**Figure 8:** Heat release rate evolution

Figure 9 shows the temperature evolution during the simulation. At the premixed and controlled mixing phase the temperature increases rapidly resulting in high heat release rate. Carbon dioxide $CO_2$ emissions are depicted in Figure 10. $CO_2$ emissions are resulting from complete combustion where the carbon atoms contained in the fuel are fully oxidized. They are usually not regulated by emission legislations and not considered as a harmful gas, however since they are a greenhouse gas, there is a strong requirement to reduce $CO_2$ emissions.

CO emissions are presented in Figure 11. They are a sign of incomplete combustion and are predominantly dependent on the equivalence ratio and temperature. CO emissions from diesel engines are typically scant because of the adequate oxygen levels (low equivalence ratio) (Kalargaris et al., 2018). Figure 12 depicts $NO_x$ emissions. In diesel engines, the mechanism that produces the majority of $NO_x$ is the thermal mechanism due to the elevated temperature and high oxygen availability.

Figure 13 and Figure 14 present respectively the variation of unburned HC and soot emissions. The HC emissions in the exhaust are mainly due to the under-mixing or over-leaning (bulk-quenching) zones and wall flame-quenching (Heywood, 1988; Mendez et al., 2009). HC and soot emissions increase strongly during the premixed combustion period reaching their peak at the end of this stage and decrease to reach the minimum at the end of the mixing-controlled combustion phase, at the same phase $NO_x$ and $CO_2$ emissions reach their constant peak at an advanced stage of the mixing-controlled combustion phase.

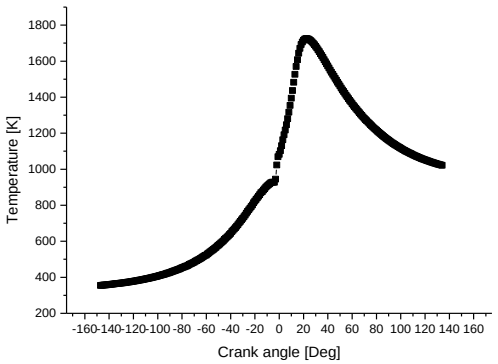


**Figure 9:** In-cylinder average temperature

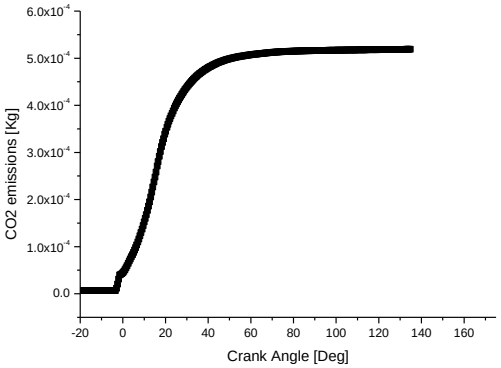


**Figure 10:** In-cylinder CO2 evolution

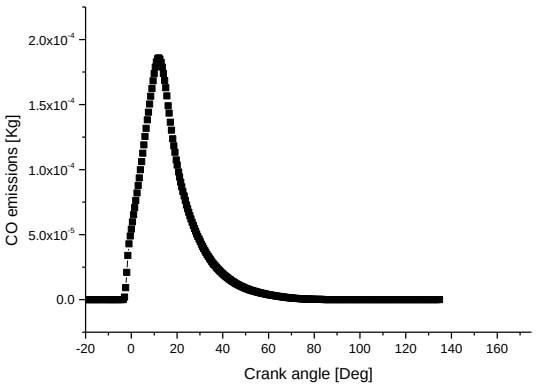


**Figure 11:** In-cylinder CO evolution

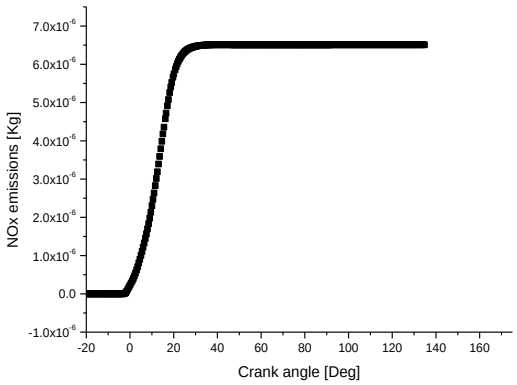


**Figure 12:** In-cylinder $NO_x$ evolution

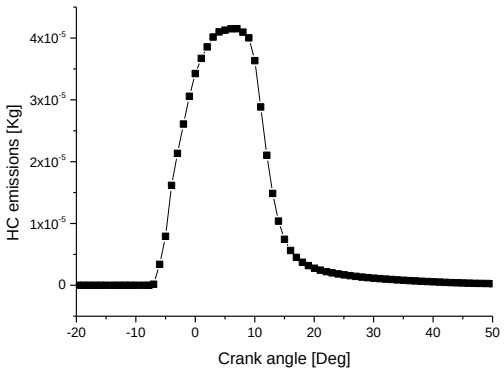


**Figure 13:** In-cylinder HC evolution

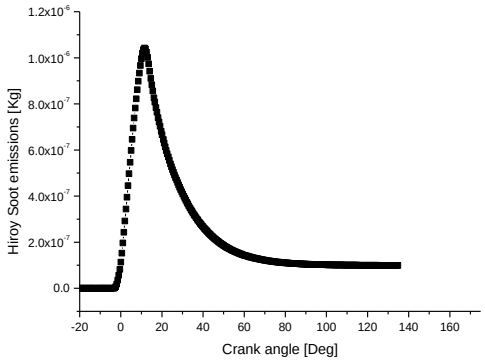


**Figure 14:** In-cylinder soot evolution

Figure 15 shows the different views of temperature, $NO_x$, CO, $CO_2$ and soot distribution for +10, +20 and +37 CAD ATDC. Previous studies (Ferguson & Kirkpatrick, 2015; Heywood, 1988; Khatir & Liazid, 2013) have reported that the greater part of the heat release form the combustion process occurs during the CO oxidation. CO emissions are mainly formed in locally rich air/fuel mixture where O2 is insufficient to completely convert all carbon fuel to $CO_2$. (Ferguson & Kirkpatrick, 2015). Figure 15 shows clearly this interaction, especially at +10 CAD ATDC. The high levels of CO are produced near the wall boundary due to the incomplete combustion resulting from low temperature at the cylinder wall.

Nitrogen oxides ($NO_x$) are composed of NO and $NO_2$. They are produced from the disassociation of $N_2$ and $O_2$ into their atomic states and subsequent reactions between them. The thermal mechanism is the major chemical mechanism that produces $NO_x$ under high temperature conditions. Figure 15 shows that NO emissions are formed during the combustion at high-temperature regions especially behind and inside the flame front. Since the volume of the high-temperature burned gases is much larger at +37 CAD ATDC, the emissions of $NO_x$ are higher than those formed at +10 and +20 CAD ATDC. With AMR and embedding around the nozzle being used, the prediction of CO, NO and soot formation can be efficiency achieved. The reason for this is that the refinement process results in high peak gas phase velocities. If this high gas phases velocities are not handled, the high drop/gas relative velocities may result. This should increase the break-up rate and therefore reduce the penetration.

The use of the refinement process reduces the drop/gas relative velocities because the gas velocity is computed accurately for the small cell size. This is very beneficial for enhancing the mixing process. As the mixing is enhanced, a high prediction of the pressure, temperature, heat release and emissions is achieved. It's important to note that the embedding is important as AMR is used, especially the embedding around the nozzle. Indeed, to save the computational time, AMR is activated at -10 CAD ATDC, that means 1 CAD before the injection. If the embedded around the nozzle is not activated, it may take too long for the AMR algorithm to detect the need for additional cells, and therefore some of the spray/gas problems may occur (Richards et al., 2008). The use of embedded around the boundary and around the nozzle before the injection with a conjunction with AMR would enhance the results for both mean and cell-by-cell results.

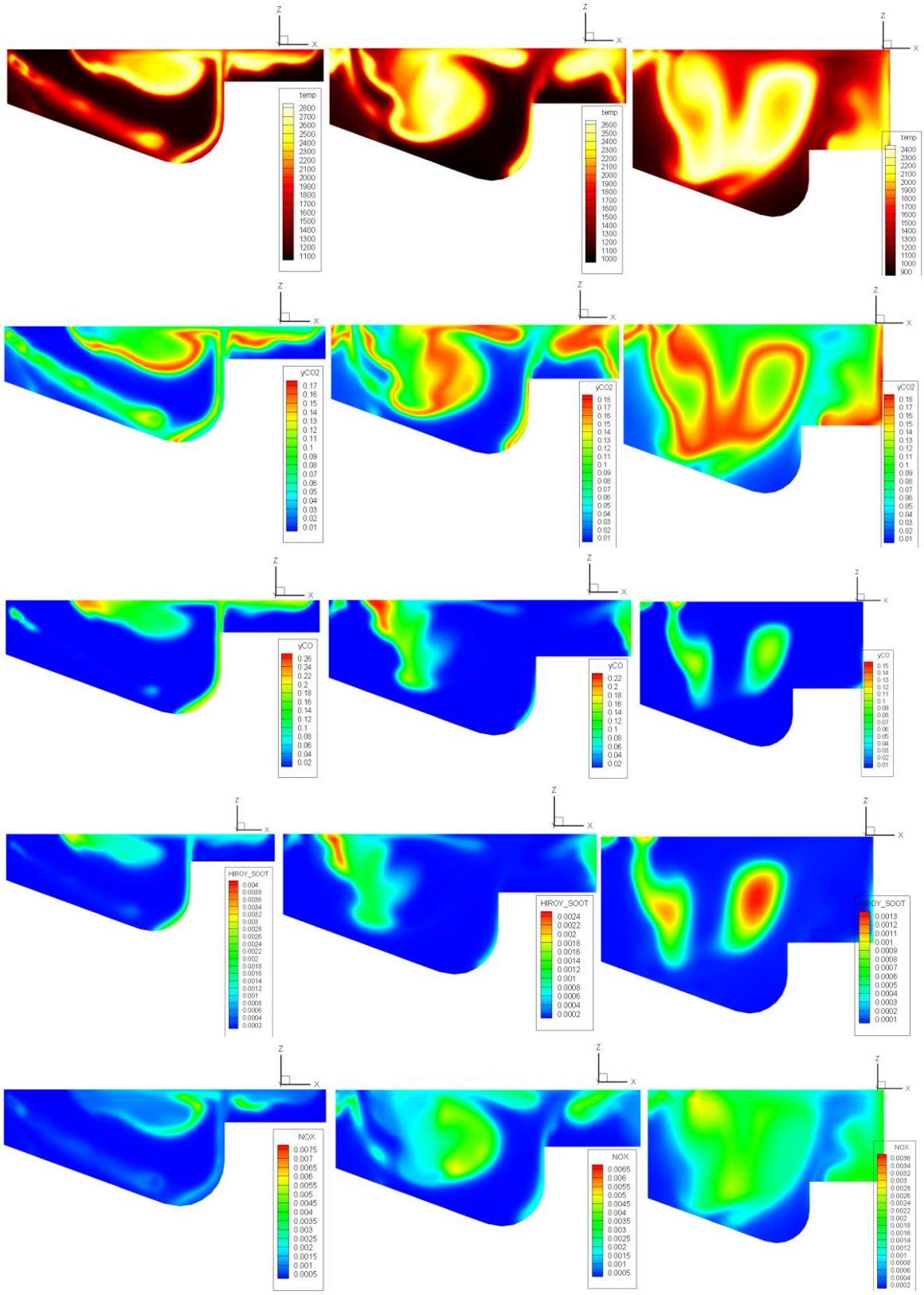


**Figure 15:** Distribution of temperature, and emissions (CO, $CO_2$, and $NO_x$) for +10, +20 and +37 CAD ATDC

## 5.0 CONCLUSION

CONVERGE code was used to study the combustion behavior in a DI engine using AMR in conjunction with an embedding around the boundary and nozzle. The mesh control should be applied during the simulation by refining automatically the grid in the regions where the flow is critical to resolve. This allows the handling of high gas velocities which enhances both the penetration of the spray and mixing. This results in high pressure, temperature and species predication. At the same time the use of AMR should be done with a conjunction with the embedding around the nozzle because this makes easy for AMR to predict where and when additional cells should be refined. The results of this simulation suggest the use of AMR for a refined grid and embedding especially around the nozzles to well investigate the combustion in ICE.

## ABBREVIATIONS

**AMR** - Adaptive Mesh Refinement
**CAD** - Crank Angle Degree
**CAD ATDC** - Crank Angle Degree After Top Dead Centre
**CAD BTDC** - Crank Angle Degree Before Top Dead Centre
**CO** - Carbon Monoxide
**$CO_2$** - Carbon Dioxide
**CTC** - Characteristic Time-scale Combustion Model
**HC** - Hydrocarbons
**HR** - Heat Release
**ICE** - Internal Combustion Engine
**IEA** - International Energy Agency
**$NO_x$** - Nitrogen Oxides
**Rpm** - Revolution per Minute
**TDC** - Top Dead Centre

## ACKNOWLEDGEMENTS

This work has been carried out at LTE laboratory with the collaboration of Convergent Science Inc. We wish to express our deep consideration to Convergent Science Inc. team for their cooperation and assistance.

## REFERENCES

Abraham, J., Bracco, F., & Reitz, R. (1985). Comparisons of computed and measured premixed charge engine combustion. *Combustion and Flame*, *60*(3), 309-322.

Amsden, D. C., & Amsden, A. A. (1993). The KIVA story: A paradigm of technology transfer. *IEEE Transactions on Professional Communication*, *36*(4), 190-195.

Atmaca, M., Girgin, İ., & Ezgi, C. (2016). CFD modeling of a diesel evaporator used in fuel cell systems. *International Journal of Hydrogen Energy*, *41*(14), 6004-6012. doi:10.1016/j.ijhydene.2016.02.122

Bousbaa, H., Sary, A., Tazerout, M., & Liazid, A. (2012). Investigations on a compression ignition engine using animal fats and vegetable oil as fuels. *Journal of Energy Resources Technology*, *134*(2), 022202, 11 p. doi:10.1115/1.4005660

Ferguson, C. R., & Kirkpatrick, A. T. (2015). *Internal combustion engines: Applied thermosciences*. Canada: John Wiley & Sons.

Frigo, S., Seggiani, M., Puccini, M., & Vitolo, S. (2014). Liquid fuel production from waste tyre pyrolysis and its utilisation in a diesel engine. *Fuel*, *116*, 399-408. doi:https://doi.org/10.1016/j.fuel.2013.08.044

Geng, P., Cao, E., Tan, Q., & Wei, L. (2016). Effects of alternative fuels on the combustion characteristics and emission products from diesel engines: A review. *Renewable and Sustainable Energy Reviews*, *71*(C), 523-534.

Guo, C., Song, Y., Feng, H., Zuo, Z., Jia, B., Zhang, Z., & Roskilly, A. P. (2018). Effect of fuel injection characteristics on the performance of a free-piston diesel engine linear generator: CFD simulation and experimental results. *Energy Conversion and Management*, *160*, 302-312. doi:10.1016/j.enconman.2018.01.052

Halstead, M., Kirsch, L., & Quinn, C. (1977). The autoignition of hydrocarbon fuels at high temperatures and pressures—fitting of a mathematical model. *Combustion and Flame*, *30*, 45-60.

Han, Z., & Reitz, R. D. (1995). Turbulence modeling of internal combustion engines using RNG κ-ε models. *Combustion Science and Technology*, *106*(4-6), 267-295.

Heywood, J. B. (1988). Internal combustion engine fundamentals (vol. 930): New York: McGraw-Hill.

Huang, M., Gowdagiri, S., Cesari, X. M., & Oehlschlaeger, M. A. (2016). Diesel engine CFD simulations: Influence of fuel variability on ignition delay. *Fuel*, *181*, 170-177.

Jafari, M., Parhizkar, M. J., Amani, E., & Naderan, H. (2016). Inclusion of entropy generation minimization in multi-objective CFD optimization of diesel engines. *Energy*, *114*, 526-541. doi:10.1016/j.energy.2016.08.026

Jiaqiang, E., Pham, M., Zhao, D., Deng, Y., Le, D., Zuo, W., Zhu, H., Liu, T., Peng, Q., & Zhang, Z. (2017). Effect of different technologies on combustion and emissions of the diesel engine fueled with biodiesel: A review. *Renewable and Sustainable Energy Reviews*, *80*, 620-647.

Kalargaris, I., Tian, G., & Gu, S. (2017). Combustion, performance and emission analysis of a DI diesel engine using plastic pyrolysis oil. *Fuel Processing Technology*, *157*, 108-115. doi:https://doi.org/10.1016/j.fuproc.2016.11.016

Kalargaris, I., Tian, G., & Gu, S. (2018). Experimental characterisation of a diesel engine running on polypropylene oils produced at different pyrolysis temperatures. *Fuel*, *211*, 797-803. doi:10.1016/j.fuel.2017.09.101

Khatir, N., & Liazid, A. (2013). Numerical investigation on combustion behaviors of direct-injection spark ignition engine fueled with CNG-hydrogen blends. *International Review of Mechanical Engineering (IREME)*, *7*(4), 652-663.

Kong, S.-C., Han, Z., & Reitz, R. D. (1995). The development and application of a diesel ignition and combustion model for multidimensional engine simulation. SAE Technical Paper 950278, Retrieved from https://doi.org/10.4271/950278

Lakshminarayanan, P., & Aghav, Y. V. (2010). *Modelling diesel combustion*. Netherlands: Springer Science & Business Media B.V..

Li, Y., Li, H., Guo, H., Li, Y., & Yao, M. (2017). A numerical investigation on methane combustion and emissions from a natural gas-diesel dual fuel engine using CFD model. *Applied Energy, 205*, 153-162. doi:10.1016/j.apenergy.2017.07.071

Masoudi, N., & Zaccour, G. (2017). Adapting to climate change: Is cooperation good for the environment? *Economics Letters*, *153*, 1-5. doi:https://doi.org/10.1016/j.econlet.2017.01.018

Maurya, R. K., & Mishra, P. (2017). Parametric investigation on combustion and emissions characteristics of a dual fuel (natural gas port injection and diesel pilot injection) engine using 0-D SRM and 3D CFD approach. *Fuel, 210*, 900-913. doi:10.1016/j.fuel.2017.09.021

Mendez, S., Kashdan, J. T., Bruneaux, G., Thirouard, B., & Vangraefschepe, F. (2009). Formation of unburned hydrocarbons in low temperature diesel combustion. *SAE International Journal of Engines*, *2*(2009-01-2729), 205-225. doi:https://doi.org/10.4271/2009-01-2729

Montgomery, D., & Reitz, R. D. (1996). *Six-mode cycle evaluation of the effect of EGR and multiple injections on particulate and NOx emissions from a DI diesel engine*. Paper presented at International Congress & Exposition, Detroit, MI, USA.

Ndayishimiye, P., Naima, K., Liazid, A., & Tazerout, M. (2011). Performance and emission characteristics of a DI compression ignition engine operated on PODL biofuel. *International Journal of Renewable Energy Technology*, *2*(3), 324. doi:10.1504/ijret.2011.040867

Ong, H., Mahlia, T., & Masjuki, H. (2011). A review on energy scenario and sustainable energy in Malaysia. *Renewable and Sustainable Energy Reviews*, *15*(1), 639-647.

Pandal, A., García-Oliver, J. M., Novella, R., & Pastor, J. M. (2018). A computational analysis of local flow for reacting Diesel sprays by means of an Eulerian CFD model. *International Journal of Multiphase Flow, 99*, 257-272. doi:10.1016/j.ijmultiphaseflow.2017.10.010

Petranović, Z., Bešenić, T., Vujanović, M., & Duić, N. (2017). Modelling pollutant emissions in diesel engines, influence of biofuel on pollutant formation. *Journal of Environmental Management, 203*, 1038-1046. doi:https://doi.org/10.1016/j.jenvman.2017.03.033

Richards, K., Senecal, P., & Pomraning, E. (2008). CONVERGE (version 1.3). Computer Software. Middleton, WI: Convergent Science, Inc.

Shi, Y., Ge, H. -W., & Reitz, R. D. (2011). *Computational optimization of internal combustion engines*. Springer-Verlag London Limited.

Sideri, M., Berton, A., & D'Orrico, F. (2017). Assessment of the wall heat transfer in 3D-CFD in-cylinder simulations of high performance diesel engines. *Energy Procedia*, *126*, 963-970. doi:10.1016/j.egypro.2017.08.187

Silva, A. O., Monteiro, C. A. A., Souza, V. P. D., Ferreira, A. S., Jaimes, R. P., Fontoura, D. V. R., & Nunhez, J. R. (2017). Fluid dynamics and reaction assessment of diesel oil hydrotreating reactors via CFD. *Fuel Processing Technology, 166*, 17-29. doi:10.1016/j.fuproc.2017.05.002

Soni, D. K., & Gupta, R. (2016). Optimization of methanol powered diesel engine: A CFD approach. *Applied Thermal Engineering*, *106*, 390-398. doi:10.1016/j.applthermaleng.2016.06.026

Wallington, T., Lambert, C., & Ruona, W. (2013). Diesel vehicles and sustainable mobility in the US. *Energy Policy*, *54*, 47-53.

Xin, J., Montgomery, D., Han, Z., & Reitz, R. (1997). Multidimensional modeling of combustion for a six-mode emissions test cycle on a DI diesel engine. *Journal of Engineering for Gas Turbines and Power, 119*(3), 683-691.